



Unraveling the relevance of the polyadenylation factor EhCFIm25 in *Entamoeba histolytica* through proteomic analysis

América Itzallana Salgado-Martínez¹, Rodolfo Gamaliel Avila-Bonilla¹ , Esther Ramírez-Moreno¹, Carlos Alberto Castañón-Sánchez², César López-Camarillo³ and Laurence A. Marchat¹ 

¹ Laboratorio de Biomedicina Molecular II, ENMH, Instituto Politécnico Nacional, Mexico City, Mexico

² Hospital Regional de Alta Especialidad de Oaxaca, Mexico

³ Posgrado en Ciencias Genómicas, Universidad Autónoma de la Ciudad de México (UACM), Mexico

Keywords

CFIm25 silencing; *Entamoeba histolytica*; polyadenylation; proteomics; virulence

Correspondence

L. A. Marchat, Sección de Estudios de Posgrado e Investigación, ENMH, Instituto Politécnico Nacional, Guillermo Massieu Helguera 239, Fracc. La Escalera, Ticoman, C.P. 07320, Ciudad de México, México
Tel: +52 55 5729 6300 ext. 55543
E-mail: lmarchat@gmail.com;
lmarchat@ipn.mx

(Received 26 May 2021, revised 6 August 2021, accepted 2 September 2021)

doi:10.1002/2211-5463.13287

Edited by Alberto Alape-Girón

We recently reported that silencing of the polyadenylation factor EhCFIm25 in *Entamoeba histolytica*, the protozoan which causes human amoebiasis, affects trophozoite proliferation, death, and virulence, suggesting that EhCFIm25 may have potential as a new biochemical target. Here, we performed a shotgun proteomic analysis to identify modulated proteins that could explain this phenotype. Data are available via ProteomeXchange with identifier PXD027784. Our results revealed changes in the abundance of 75 proteins. Interestingly, STRING analysis, functional GO-term annotations, KEGG analyses, and literature review showed that modulated proteins are mainly related to glycolysis and carbon metabolism, cytoskeleton dynamics, and parasite virulence, as well as gene expression and protein modifications. Further studies are needed to confirm the hypotheses emerging from this proteomic analysis, to thereby acquire a comprehensive view of the molecular mechanisms involved.

Gene expression regulation is a key event for eukaryotic cell biology and survival, allowing organisms to adapt to stress, extracellular stimuli, and cell–cell communication by adjusting protein synthesis. After gene transcription by RNA polymerase II (RNA Pol II) in the nucleus, pre-mRNA molecules are modified by 5'

end capping, splicing, and 3'-end polyadenylation to generate mature transcripts that travel to cytoplasm to be translated to proteins. These different regulatory steps in gene expression have been studied in *Entamoeba histolytica*, the protozoan parasite responsible for amebic dysentery and amebic liver abscess that

Abbreviations

3' UTR, 3' untranslated region; ABP, actin-binding protein; ACD, acetyl-CoA synthetase_ putative; ADHE, aldehyde-alcohol dehydrogenase; ALDO, aldolase; CAP, cyclase-associated protein; CF, cleavage factor; CPBF, cysteine protease-binding protein family; CPSF, cleavage and polyadenylation specificity factor; CstF, cleavage stimulation factor; dsRNA, double-stranded RNA; ENO, enolase_ putative; G3PDH, glycerol-3-phosphate dehydrogenase; GAPDH, glyceraldehyde 3-phosphate dehydrogenase; GPP/GK, glycerol-3-phosphate phosphatase/glycerol kinase; HK, hexokinase; HPI, phosphoglucose isomerase; MDH, malate dehydrogenase; ME, malic enzyme; PABP, poly(A) binding protein; PAP, poly(A) polymerase; PEPCK3, phosphoenolpyruvate carboxykinase; PFKm, phosphofructokinase; PFOR, pyruvate: ferredoxin oxidoreductase; PGAM, phosphoglycerate mutase; PGK, phosphoglycerate kinase; PK/PPDK, pyruvate_ phosphate dikinase; PPI-PFK/PFK, pyrophosphate-fructose 6-phosphate 1-phosphotransferase; RNA Pol II, RNA polymerase II; SOD, superoxide dismutase; TPI, triosephosphate isomerase.

represents one of the major leading causes of death from parasitic diseases worldwide, mainly in developing countries [1]. Relevant DNA motifs in promoters and several transcription factors have been reported; capping has not been described yet, but most of the main components of splicing and polyadenylation machineries found in higher eukaryotic cells, have been identified [2]. Our group reported that *E. histolytica* presents the six subunits of the cleavage and polyadenylation specificity factor (CPSF160, CPSF100, CPSF73, CPSF30, Fip1, and WDR33), but only two of the three subunits of the cleavage stimulation factor (CstF77 and CstF64); it has both CLP1 and PCF11 subunits of the cleavage factor IIm (CFIIm), but only the small 25 kDa subunit of the CFIIm; the poly(A) polymerase (PAP), the poly(A) binding protein (PABP), RBPP6, and PP1a were also found [3].

In humans, CFIImI is a heterotetramer complex with two 25 kDa subunits bound to a dimer of larger subunits (59 or 68 kDa). Notably, CFIIm25 is essential for polyadenylation factor recruitment, poly(A) site selection, pre-mRNA cleavage, and poly(A) tail synthesis [4–7]. The fact that the 25 kDa subunit is the only CFIIm component identified in *E. histolytica* suggests that mRNA polyadenylation could involve a different mechanism in this parasite, and EhCFIm25 could have a central role in this event. Molecular characterization of EhCFIm25 confirmed that it is a Nudix protein although three of the four glutamate residues (E154, E157, and E158) in the conserved Nudix box are replaced by lysine, and the last glycine residue (G160) is substituted by the hydrophilic residue serine. As the human protein, EhCFIm25 interacts with EhPAP [8], but also with the transcriptional coactivator EhPC4 (J. D. Ospina-Villa, our unpublished data) related to virulence, DNA replication, and multinucleation in *E. histolytica* [9,10]. Although three-dimensional structure prediction indicates the absence of a classical RNA-binding domain, EhCFIm25 can bind the 3' untranslated region (3' UTR) of *E. histolytica* transcripts through the participation of the conserved Leu135 and Tyr236 residues [11,12]. By using the SELEX strategy, we isolated two RNA aptamers that contain the GUUG motif recognized by EhCFIm25. Importantly, EhCFIm25 sequester by aptamers, rapidly induced parasite death, which confirms that targeting the polyadenylation process, namely EhCFIm25, represents an effective strategy for controlling *E. histolytica* [13]. On the other hand, EhCFIm25 silencing produced a significant acceleration in parasite proliferation and cell death; moreover, cells were larger and multinucleated, and their ability to move and phagocyte erythrocytes was significantly reduced, indicating loss of

virulence. Additionally, functional experiments showed that EhCFIm25 controls the selection of the distal poly(A) site in mRNA 3'UTR [14]. However, the relationships between EhCFIm25 inhibition and these phenotypical characteristics remain unknown. Here, we performed a shotgun proteomic analysis to evidence changes in protein expression that can explain the observed phenotype.

Materials and methods

Microorganisms

Entamoeba histolytica trophozoites (strain HMI:IMSS) were grown in aerobic and axenic conditions at 37 °C in TYI-S-33 medium with 20% adult bovine serum, 100 U·mL⁻¹ penicillin, and 100 µg·mL⁻¹ streptomycin [15]. *Escherichia coli* strain HT115 (rnc14:DTn10) was grown at 37 °C in LB and 2YT broth for plasmid pL4440-EhCFIm25 maintenance and EhCFIm25-dsRNA expression, respectively, supplemented with ampicillin (100 mg·mL⁻¹) and tetracycline (10 mg·mL⁻¹) [14].

EhCFIm25 gene silencing

Double-stranded RNA (dsRNA)-based *EhCFIm25* gene silencing was performed as described [14]. Briefly, *E. histolytica* trophozoites (5.0×10^4) were grown for 4 days in TYI-S-33 complete medium in the presence of *EhCFIm25*-dsRNA molecules (100 µg·mL⁻¹) obtained from *E. coli* HT115 (rnc14:DTn10) cells transformed with the pL4440-*EhCFIm25* plasmid. Every day, a 10 µL aliquot of culture was taken to determine parasite number in a Neubauer chamber and living cells stained by Trypan blue. Experiments were performed twice in triplicate, and results were expressed as mean ± SD. Trophozoites growing in standard conditions (without dsRNA) and treated with *gfp*-dsRNA were used as controls. Data corresponding to the *EhCFIm25*-dsRNA condition were compared with both control conditions using the two-way ANOVA test. $P < 0.05$ was considered as statistically significant.

RNA and protein isolation

Total proteins and RNA of *E. histolytica* trophozoites treated with *EhCFIm25*-dsRNA and control cells (day 4) were obtained by the TRIzol reagent (Invitrogen) according to manufacturer's instructions. Protein quality and amount were verified by 10% SDS/PAGE and the Bradford method before being used in Mass spectrometry assays. RNA integrity and concentration were assessed by agarose gel electrophoresis and spectrophotometric analysis in a spectrophotometer (NanoReady Touch, Hangzhou Lifereal Biotechnology). RNA was used in Real-Time qRT-PCR to

assess inhibition of *EhCFIm25* mRNA expression and validate proteomic data as described below.

Mass spectrometry analysis LC-ESI-HDMSE

The volume corresponding to 150 µg total proteins obtained from the three culture conditions was delivered to the Laboratorio Nacional de Servicios Experimentales (LaNSE), CINVESTAV (Mexico), for protein identification and absolute quantitation by mass spectrometry analysis LC-ESI-HDMSE as described [16,17]. Raw files containing MS and MS/MS spectra were deconvoluted, compared, and quantified by PROTEINLYNX GLOBAL SERVER (PLGS) v3.0.3 software against *E. histolytica* (Strain: ATCC 30459/HM-1:IMSS, downloaded from UniProt, 7959 protein sequences, 3 February 2021) concatenated with reverse database. Workflow parameters were included as described [17]. [All protein identifications reported had a percentage of $\geq 95\%$ reliability (protein autocurate green)]. Full data are included in Table S1.

Data analysis and bioinformatics

Protein amounts (fmol) in trophozoites treated with *EhCFIm25*-dsRNA were compared with trophozoites treated with *gfp*-dsRNA and nontreated control cells; all data were expressed as a base 2 logarithm [18]. Protein abundance changes were used to construct a hierarchical clustering (Euclidean distance) by the heatmapper program (<http://www.heatmapper.ca>). Proteins displaying at least ± 1.0 absolute fold change in both comparisons, *EhCFIm25*-dsRNA vs. *gfp*-dsRNA and *EhCFIm25*-dsRNA vs. nontreated cells, were considered as differentially expressed and selected for further analyses; proteins that were detected in control cells but not in the *EhCFIm25*-dsRNA condition were also considered in the study. Selected proteins were used Gene Ontology (GO) enrichment analysis. The GO terms and biochemical pathways of proteins were obtained using DAVID v6.8 (<https://david.ncifcrf.gov/>) and corroborated in AmoebaDB database (<https://amoebadb.org/amoeba/app/>), UniProt database (<https://www.uniprot.org/>), and KEGG PATHWAY database (<https://www.genome.jp/kegg/pathway.html>). All data were visualized using the CytoScape tools software (<https://cytoscape.org/>). Additionally, modulated proteins were submitted to STRING analysis using the MCL clustering tool (<https://string-db.org/>).

Real-Time qRT-PCR (Real-Time Quantitative Reverse Transcription-PCR)

Total RNA was used to synthesize cDNA using the SuperScript III Reverse Transcriptase (Invitrogen) according to manufacturer's instructions in a GeneQ Thermal Cycler (BIOER, Hangzhou, China). The qPCR assay was

completed using SensiFAST™ SYBR Hi-ROX (Bioline) with specific primers for selected genes as follows: EhCFIm25: sense 5'-TGGAGAAGATGATCCTGTTGAAG-3' and antisense 5'-TCTTTGACTTGACTTACATGAACTG-3' primers [14]; pyruvate phosphate dikinase (PPDK): sense 5'-CAGC TACTGGTGTGTTTGTTCAC-3' and antisense 5'-GATCT GCATCTTCTGCCATCT-3' primers; pyruvate:ferredoxin oxidoreductase (PFOR): sense 5'-CCCAATTACACCATC ATCACC-3' and antisense 5'-ATGCTCCAGCTTCACCTT CC-3' primers; peroxiredoxin, putative (PRX): sense 5'-AG CATGGTGTGAAGCAGATAA-3' and antisense 5'-CCT GCTTCGACATTTAACATTCC-3' primers; acetyl-CoA synthetase, putative (ACD): sense 5'-ACAGAGGAATG CCAGCTTGT-3' and antisense 5'-GGTTGGATGACGA GGTGAG-3' primers; actin-like protein, putative (ARP2/3): sense 5'-TTCCCAACAGCCATCTTTCCA-3' and antisense 5'-GCAGCTGCTTCATCTCCAAAC-3' primers; myosin heavy chain: sense 5'-TGGGTAAAGCTGGAGCACAT-3' and antisense 5'-GTGTCCATGGGATACCTTCGT-3' primers; ubiquitin putative: sense 5'-AGGAATCCACCTGA TCAACA-3' and antisense 5'-TCTGAAAGTGTCTTTC CTTCTTCT-3' primers; PC4: sense 5'-AAAACCTCCATT TGACGGTGACAA-3' and antisense 5'-TCCTGGTTTTA ATTCTCCATCTCT-3' primers; and PAP: sense 5'-GTGC AGGAGTTGCTGATGAC-3' and antisense 5'-TGTGGT GATCGTTTTGATGGA-3' primers. The EhRNAPII gene was used for normalization (sense 5'-GATCCAACATATC CTAAAACAACA-3' and antisense 5'-TCAATTATTTTCT GACCCGTCTTC-3' primers) [19]. All reactions were performed in a StepOne real-time PCR system (Applied Biosystems) with the following cycling conditions: enzyme activation at 95 °C for 2 min, followed by 40 cycles of denaturation at 95 °C for 5 s and annealing/extension at 62 °C for 30 s. The experiment was carried out by triplicated, and the relative expression of mRNA was determined by the $2^{-\Delta\Delta C_t}$ method. Data corresponding to the *EhCFIm25*-dsRNA condition were analyzed by Prism GraphPad software using paired Student's *t*-test to compare the *EhCFIm25*-dsRNA condition with both control conditions. $P < 0.05$ was considered as statistically significant.

Results

Silencing of *EhCFIm25* by dsRNA

To evidence how the absence of EhCFIm25 affects protein expression, we first induced downregulation of *EhCFIm25* gene expression by soaking trophozoites with purified *EhCFIm25*-dsRNA as described [14]. As expected, real-time qRT-PCR assays confirmed that on day 4, *EhCFIm25* gene transcription was reduced by about 75% in parasite cultures containing *EhCFIm25*-dsRNA, when compared with *gfp*-dsRNA-treated cells and nontreated cells. Additionally, trophozoites

exhibited an accelerated proliferation from day 2 when compared with both control cells, as well as a higher number of dead cells (Fig. S1). All these observations agreed with our previous report [14] and strongly supported the downregulation of *EhCFIm25* expression following *EhCFIm25*-dsRNA soaking.

Identification of modulated proteins following *EhCFIm25* silencing

Protein extracts were obtained from *EhCFIm25*-dsRNA-treated trophozoites and both control cultures (*gfp*-dsRNA condition and nontreated cells) and analyzed by mass spectrometry analysis LC-ESI-HDMSE as described [16–18]. A total of 139 proteins (including 11 uncharacterized proteins) was identified and quantified, considering 99.9% accuracy and detection of at least two peptides for protein identification (Table S1). Hierarchical clustering evidenced that many proteins showed similar changes in abundance when comparing *EhCFIm25*-dsRNA-treated cells vs. *gfp*-dsRNA condition and nontreated cells, indicating that *EhCFIm25* silencing had an effect on the gene expression (Fig. 1). Because of the relevance of *EhCFIm25* in polyadenylation and the role of poly(A) tail in translation and mRNA stability, the absence of *EhCFIm25* probably affected mRNA turnover and translation; however, we cannot discard that the turnover of some proteins could also be changed.

Of these 139 proteins, 75 showed a significant log₂ fold change value when comparing *EhCFIm25*-dsRNA-treated cells vs. both control conditions. These included 48 less abundant proteins (comprising four uncharacterized proteins) and 12 more abundant proteins (with two uncharacterized proteins); notably, 15 proteins (including four uncharacterized proteins) were not detected in the absence of *EhCFIm25* (Fig. 2A). The four most reduced proteins were the PPI-type phosphoenolpyruvate carboxykinase 3 (C4LWQ8) (PPI-PEPCK3/PEPCK3), the pyrophosphate-fructose 6-phosphate 1-phosphotransferase (C4LZC2) (PPI-PFK/PFK), and the 3-ketoacyl-CoA synthase 4

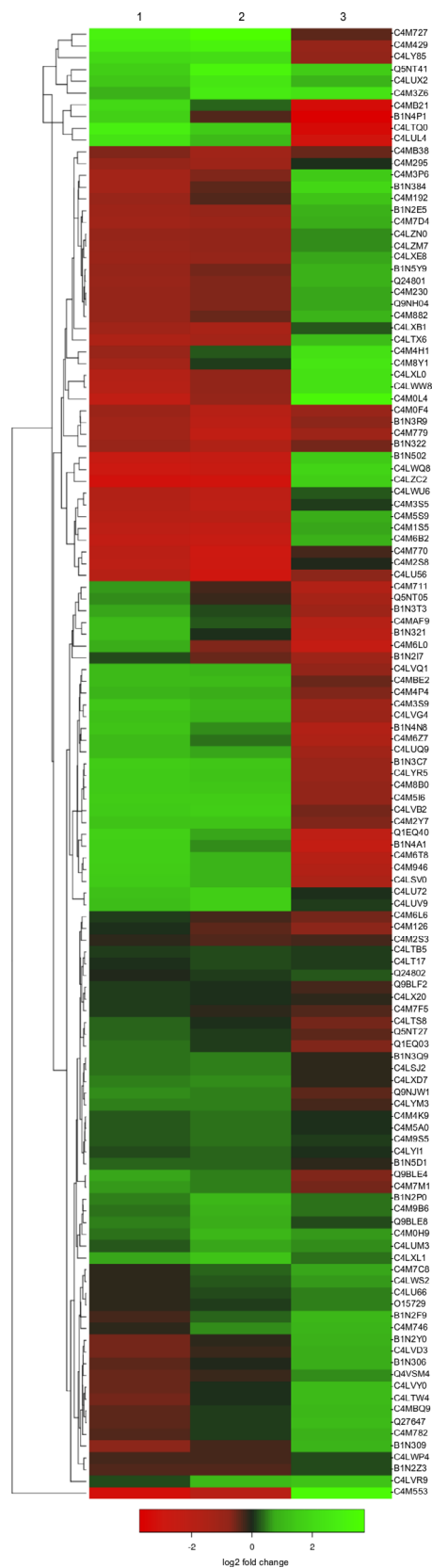


Fig. 1. Protein abundance changes in *E. histolytica* trophozoites treated with *EhCFIm25*-dsRNA and controls. The heat map shows the hierarchical clustering (Euclidean distance) of base 2 logarithm protein abundance. Lane 1, *EhCFIm25*-dsRNA-treated cells vs. *gfp*-dsRNA condition; lane 2, *EhCFIm25*-dsRNA-treated cells vs. and nontreated cells; lane 3, *gfp*-dsRNA-treated cells vs. nontreated cells. Color key: increased proteins (green); reduced proteins (red). The 15 proteins that were not detected in *EmCFIm25* silenced cells are not represented here.

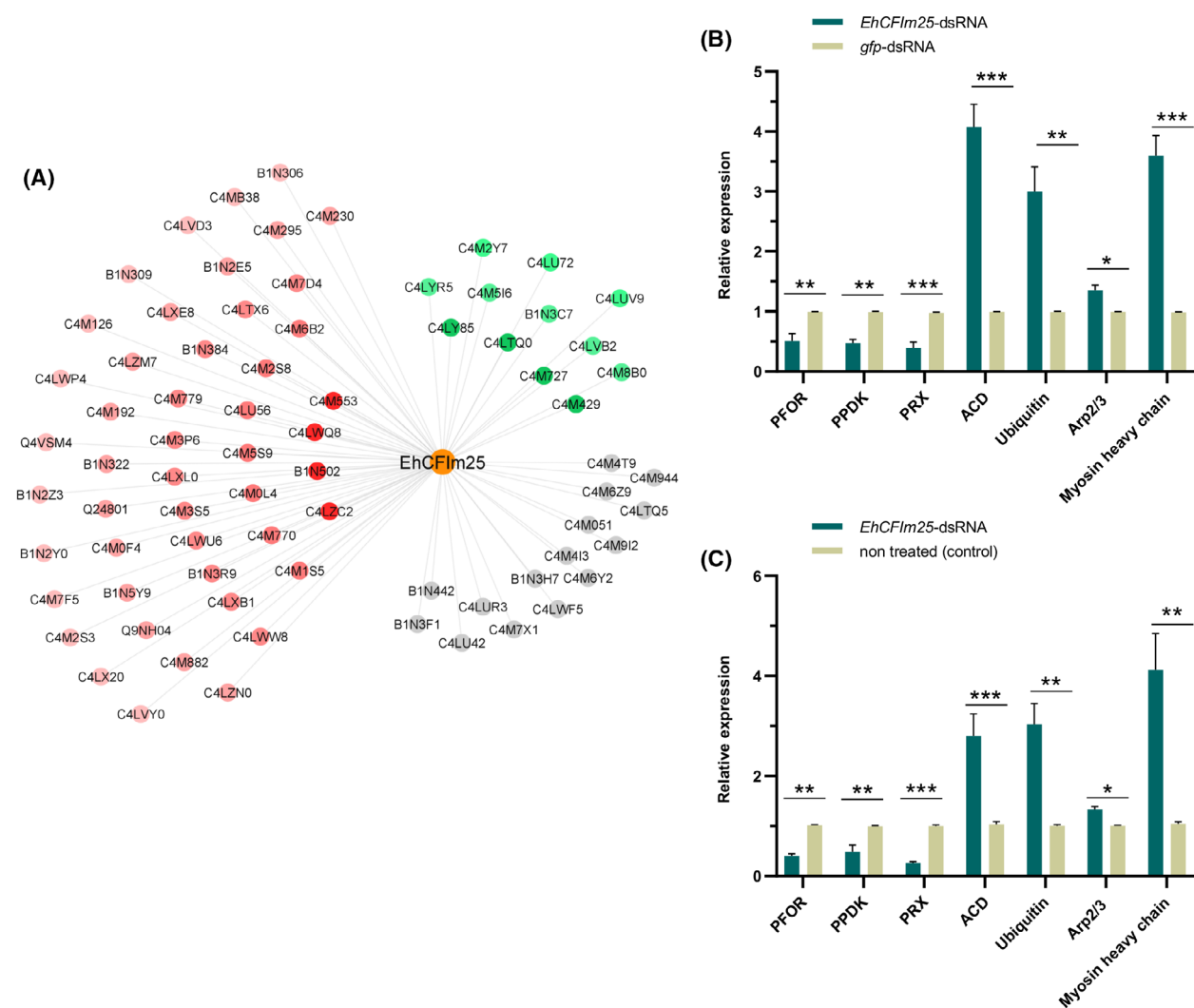


Fig. 2. *E. histolytica* proteins modulated in response to *EhCFIm25* silencing. (A) Schematic representation of proteins with significant changes in abundance following *EhCFIm25* silencing. Red, proteins in a reduced amount; green, proteins in a higher amount; gray, proteins that were not detected. The color intensity is proportional to log₂ fold change value. (B and C) Real-time quantitative reverse transcription polymerase chain reaction (real-time qRT-PCR) for seven selected genes in *EhCFIm25*-dsRNA trophozoites compared with (A) nontreated cells and (C) *gfp*-dsRNA-treated parasites. The *EhRNAPII* gene mRNA expression was determined and used as normalization control for all qRT-PCR assays. Data corresponding to the *EhCFIm25*-dsRNA condition were compared with both control conditions using the paired Student's *t*-test. ***P* < 0.01; ****P* < 0.001. *n* = 3. Error bars represent SD.

(B1N502) that are related to metabolic pathways, such as glycolysis, and lipid metabolism, respectively, as well as a leucine-rich (LRR) repeat containing protein (C4M553). On the other hand, three of the highly enriched proteins corresponded to the 60S ribosomal protein L14 (C4LTQ0), 60S ribosomal protein L27 (C4M727), and ubiquitin (C4LY85), indicating that *EhCFIm25* silencing had an impact on protein synthesis. The fourth one is an uncharacterized protein (C4M429). To validate changes in protein abundance, we selected genes corresponding to three proteins with

a reduced abundance, PFOR, PPDK, and PRX, and four proteins with an increased amount, ACD, ARP2/3, myosin heavy chain ubiquitin, and evaluated mRNA expression by real-time RT-qPCR in the three groups of trophozoites. In agreement with proteomics data, PFOR, PPDK, and PRX genes were downregulated in response to *EhCFIm25* silencing in comparison with the untreated cells and the *gfp*-dsRNA condition, while ACD, ARP2/3, and myosin heavy chain ubiquitin genes were upregulated (Fig. 2B,C). We previously showed that EhCFIm25 interacts with EhPAP and

EhPC4, two proteins involved in polyadenylation and transcription, respectively. Although these nuclear proteins did not appear in the proteomes, we investigate whether there were any changes in the mRNA expression of EhPAP and EhPC4 genes upon silencing the EhCFIm25. Results showed mRNA expression of both genes was increased in EhCFIm25-silenced trophozoites (Fig. S2).

With the aim of having a general view of the impact of change in protein abundance in *EhCFIm25*-silenced trophozoites, the identified proteins were categorized using functional GO-term annotations. The 10 uncharacterized proteins were not included since BLAST analyses failed to assign them a possible identity and function (data not shown). Many of the less abundant proteins corresponded to cellular and intracellular compartments; concerning biological process, they were mainly associated with metabolism, including metabolic process, organic substance metabolic process, and cellular metabolic process; finally, the main function was binding. Regarding proteins that were more abundant in the absence of EhCFIm25, they were mainly found as part of the ribosome and cytoplasm, and mostly related to Arp2/3 complex-mediated actin nucleation and translation; interestingly, the main molecular functions were related to binding, including RNA, ATP, and nucleotide binding, as well as ATPase activity. Lastly, proteins that were not detected in *EhCFIm25*-silenced trophozoites corresponded to cytosol and ribosome; they were mainly associated with translation and related to nucleotide and RNA binding, as well as part of the structural constituent of ribosome (Fig. 3).

KEGG analyses evidenced that four of the proteins with a reduced abundance, C4LXE8, C4M192, C4M230, and C4LVD3, have an impact on at least five biochemical pathways. They also confirmed that reduced proteins are mainly related to metabolism, namely carbon metabolism, metabolic pathways, glycolysis/gluconeogenesis, and pyruvate metabolism; they were also related to gene expression regulation by acting in spliceosome, protein processing and endoplasmic reticulum, ribosome, RNA transport, aminoacyl-tRNA biosynthesis, and biosynthesis of amino acids. Regarding proteins with an increased abundance, three proteins (C4M8B0, C4M2Y7, and C4LY85) were involved in two biochemical pathways. Regulation of actin cytoskeleton was the most affected pathway. On the other hand, three of the proteins that were not detected in *EhCFIm25*-silenced trophozoites (C4M4T9, B1N3F1, and C4M6Y2) participate in three biochemical pathways. Gene expression regulation, including RNA transport and mRNA

surveillance, spliceosome, and ribosome, was the most affected process (Fig. 4).

In order to better understand how *EhCFIm25* silencing affected *E. histolytica* trophozoites, these functional categorization analyses were completed by a STRING analysis. Interestingly, modulated proteins formed three main groups that remain interconnected through several proteins. One group correspond proteins related to metabolism including glycolysis (EHI_00070, EHI_188180, EHI_130700, EHI_009530, 051060, EHI_178960, EHI_150490), 14-3-3 proteins (EHI_098280, EHI_006810), among others, as well as heat-shock proteins (EHI_199590, EHI_052860; EHI_196940); the other corresponds to cytoskeletal proteins (EHI_110180, EHI_111050, EHI_094060, EHI_154430, and EHI_199000), and the last one is related to translation with the presence of ribosomal proteins (e.g., EHI_050130, EHI_183480, EHI_006860), aminoacyl-tRNA synthetases (such as EHI_126920 and EHI_073460), elongation factors (EHI_166810, EHI_011210), and among others (Fig. 5). Finally, manual annotation of *E. histolytica* proteins and retrieving of published literature allowed us to cluster modulated proteins into three large biological processes, that is, glycolysis and carbon metabolism, cytoskeleton dynamics and parasite virulence, and gene expression and protein modifications (Table 1).

Discussion

We previously reported that EhCFIm25 is essential for *E. histolytica* survival and virulence properties, since its silencing affected trophozoite proliferation, produced parasite death, altered cell size and nucleus number, and reduced mobility and erythrophagocytosis capacity of parasites, which prompted us to propose this polyadenylation factor as a new biochemical target in this human pathogen [14]. Our proteomic analysis revealed that the absence of EhCFIm25 produced changes in the abundance of 75 proteins. Among these, we focused on proteins related to glycolysis and carbon metabolism, cytoskeleton dynamics and parasite virulence, and gene expression and protein modifications.

EhCFIm25 silencing affects energy metabolism causing parasite death

E. histolytica trophozoites lack a functional Krebs cycle and oxidative phosphorylation enzymes and exclusively depend on an unusual PPI-dependent glycolytic pathway for ATP generation from glucose fermentation. The acetyl-CoA molecule obtained from

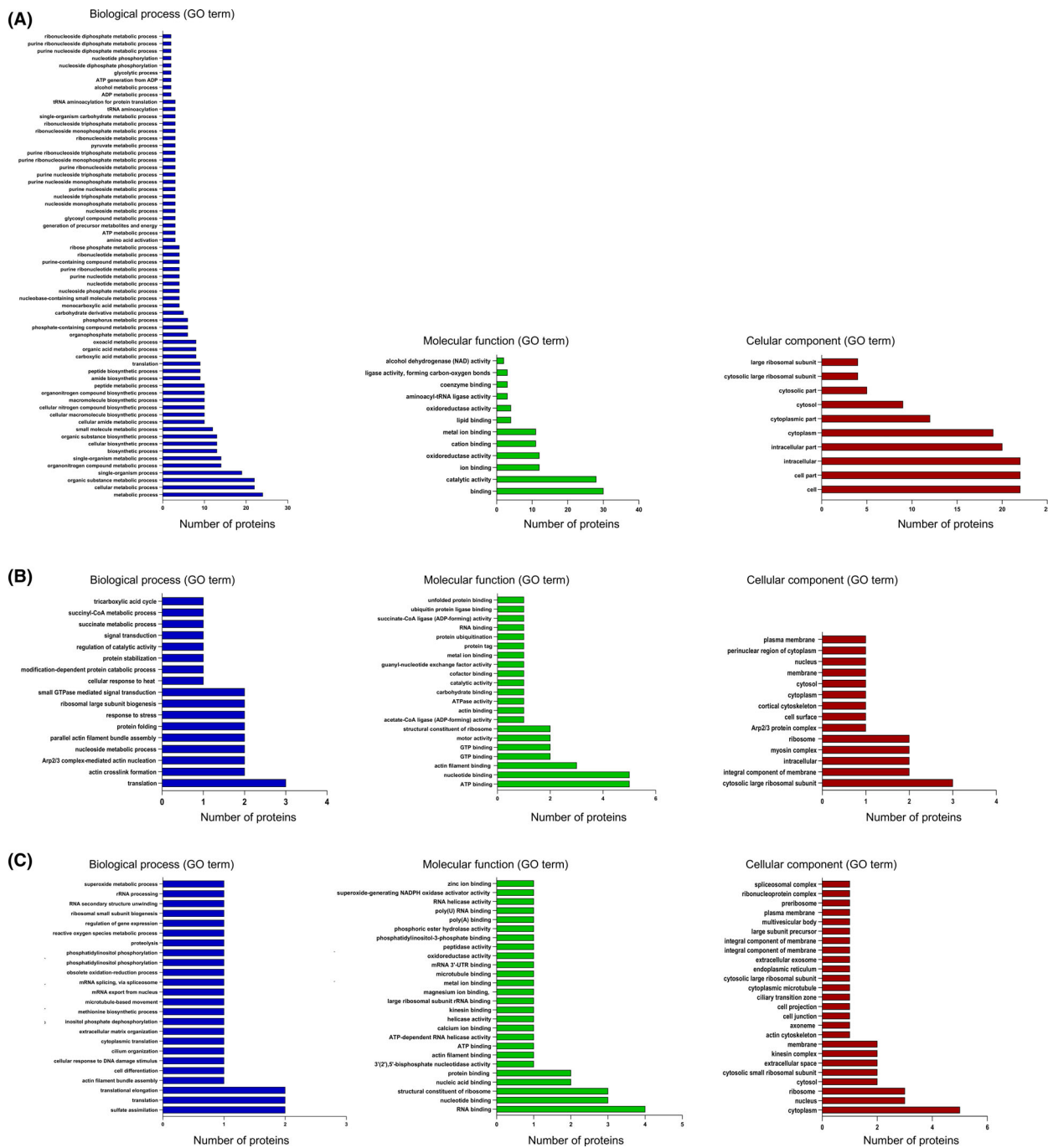


Fig. 3. Functional categorization of proteins with modulated abundance following *EhCFIm25* silencing. Proteins with a reduced abundance (A), an increased abundance (B), and proteins that were not detected (C) were classified according to cellular component, biological process, and molecular function, defined from Gene Ontology categories by DAVID.

the pyruvate end product of glycolysis can be transformed to ethanol by the aldehyde-alcohol dehydrogenase (ADHE also known as ADH2) in a two-step reaction or acetate by the ADP-forming ACD [20]. Our results evidenced the reduced abundance of

PPi_PFK/PFK (C4LZC2), phosphoglycerate kinase (C4M192) (PGK), enolase_putative (C4LXE8) (ENO), PK/PPDK (Q24801), PFOR (C4LTX6), and ADHE (C4M230), which results in an overall reduction in ethanol and ATP production. Other glycolysis-related

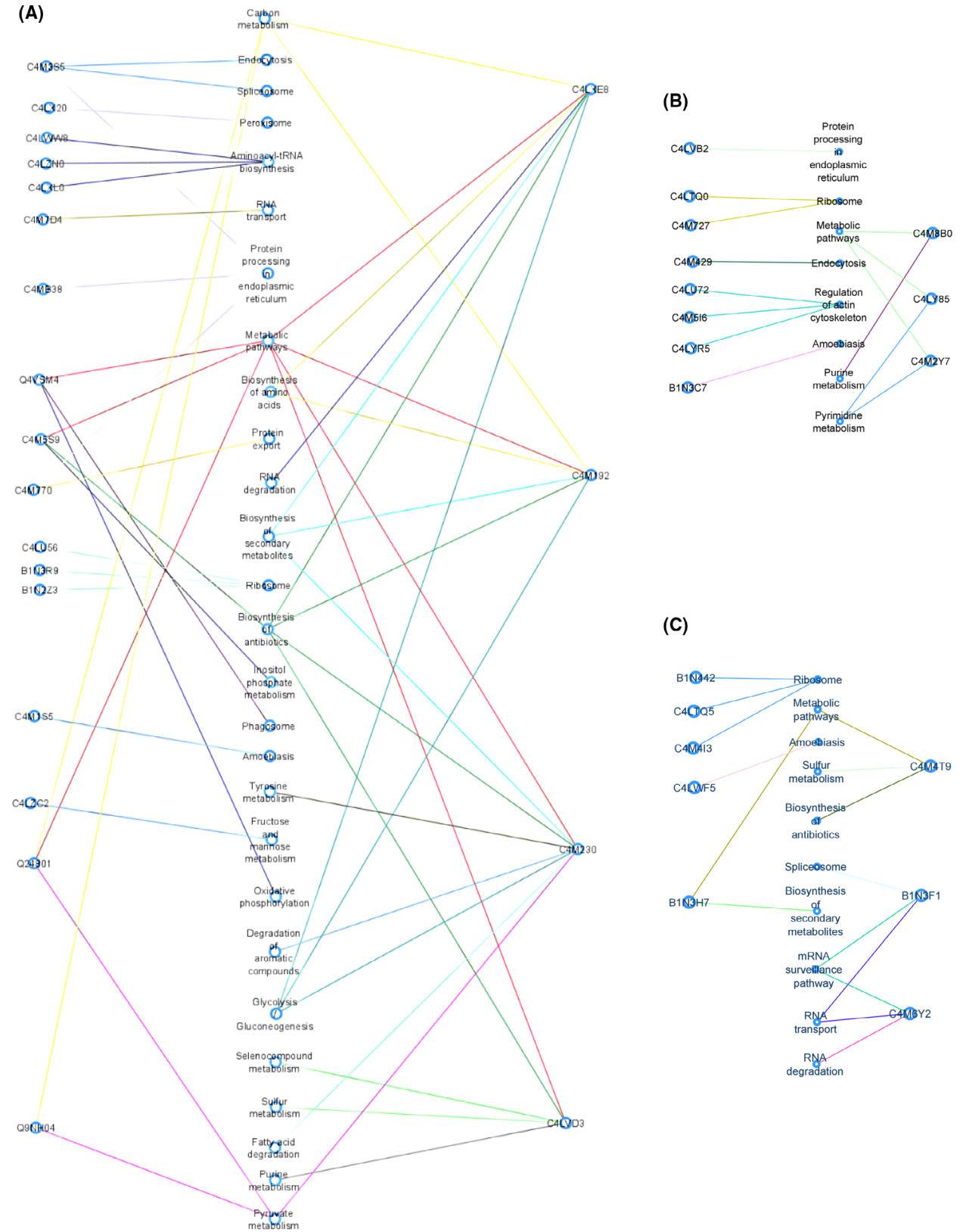


Fig. 4. KEGG pathways associated with proteins with a reduced abundance (A), an increased abundance (B), and proteins that were not detected (C) following *EhCFIm25* silencing.

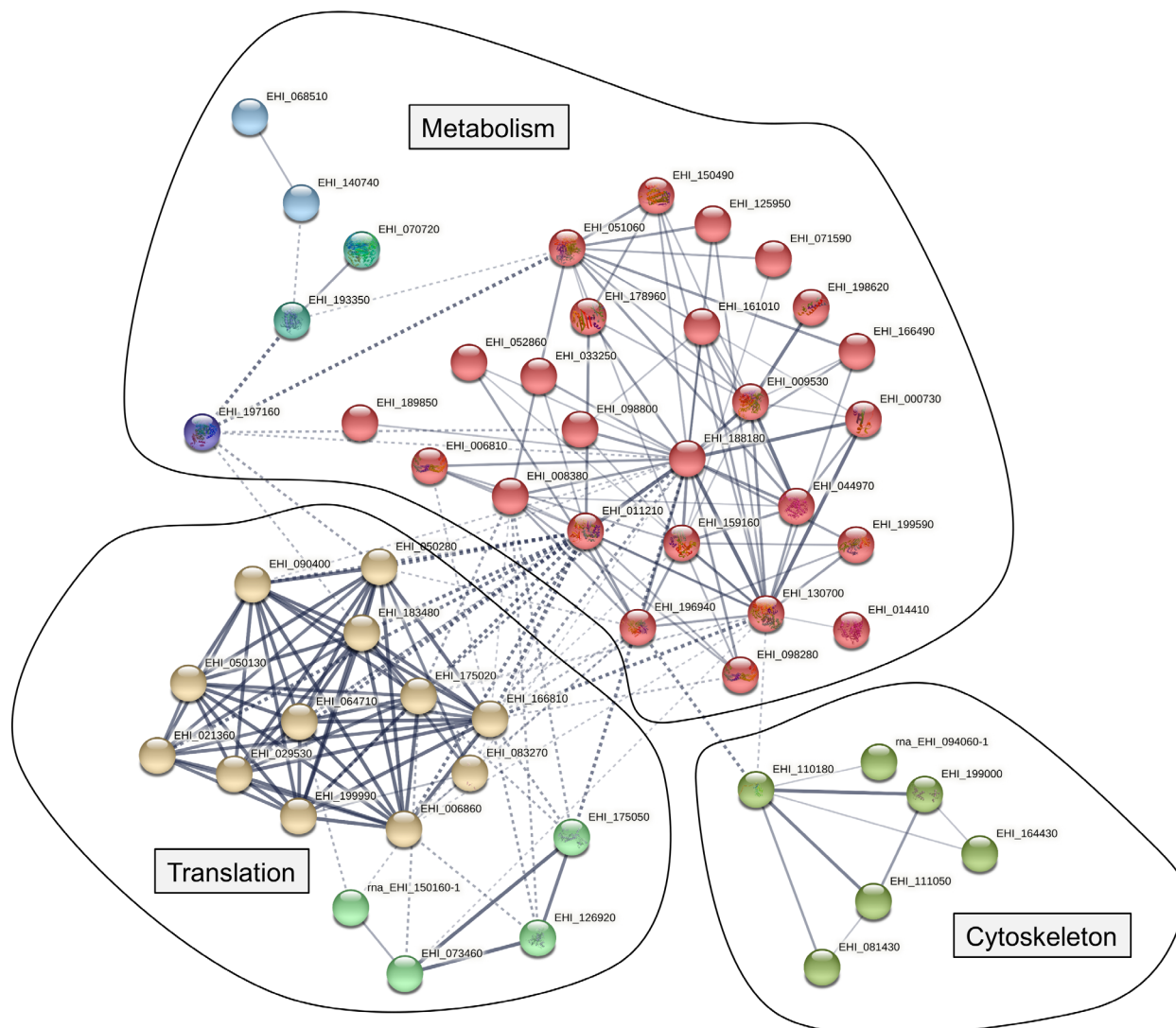


Fig. 5. Protein–protein interaction network visualized by STRING. Colored nodes correspond to query proteins and first shell of interactions. The color saturation of the edges represents the confidence score of the association between modulated proteins

enzymes were also affected, such as PPi-type phosphoenolpyruvate carboxykinase 3 (C4LWQ8) (PPi-PEPCK3), malic enzyme (Q9NH04) (ME), and malate dehydrogenase_putative (B1N2Y0) (MDH) that control the PEP-oxaloacetate-malate-pyruvate cycle, the L-myo-inositol-1-phosphate synthase (C4M5S9) that catalyzes the conversion of glucose 6-phosphate to 1-l-myo-inositol-1-phosphate, and the anaerobic glycerol-3-phosphate dehydrogenase subunit A_putative (B1N3H7) (G3PDH) that converts glycerol-3-phosphate to dihydroxyacetone phosphate [21]. Interestingly, the increased abundance of the acetyl-CoA synthetase_putative (C4LUV9) (ACD) and the reduced amount of bifunctional ADHE (C4M230), and

C4LVY0 and C4M7F5, two putative alcohol dehydrogenases of 42 kDa and 46 kDa, respectively, that did not correspond to the reported ADH1 (39 kDa) and ADH3 (43 kDa), suggested that parasites direct the last steps of glycolysis to the conversion of acetyl-CoA into acetate with the production of ATP in an attempt to restore, at least partially, the lack of energy that results from downregulation of upstream glycolytic enzymes (Fig. 6). However, energy deficiency is likely the main cause of parasite death following *EhCFIm25* silencing. In agreement with this assumption, it has been reported that ADHE activity is an important control point for the glycolytic flux and its inhibition can decrease the parasite energy load and survival [22].

Table 1. Modulated proteins in *EhCFIm25*-silenced trophozoites

Gene ID	UniProt	NCBI	Protein description	<i>EhCFIm25</i> - dsRNA vs nontreated (control) (log2 fold change)	<i>EhCFIm25</i> - dsRNA vs <i>gfp</i> -dsRNA (log2 fold change)	<i>gfp</i> -dsRNA vs nontreated (control) (log2 fold change)
Glycolysis and carbon metabolism						
Increased						
EHI_178960	C4LUV9	XP_656290.1	ACD	1.571976609	1.838014699	0.26603809
Reduced						
EHI_000730	C4LZC2	XP_653173.1	PPi_PFK	-8.953922033	-6.824743753	2.129178281
EHI_188180	C4M192	XP_653686.1	PGK	-3.53422426	-1.70492415	1.82930011
EHI_130700	C4LXE8	XP_649161.1	ENO	-3.664724348	-2.623408105	1.041316242
EHI_051060	C4LTX6	XP_657019.2	PFOR	-5.023063656	-3.386220638	1.636843018
EHI_009530	Q24801	XP_657332.1	PK/PPDK	-3.443328065	-2.212267448	1.231060617
EHI_150490	C4M230	XP_652300.1	ADHE	-3.338295165	-2.276880037	1.061415128
EHI_125950	C4LVY0	XP_650419.1	Alcohol dehydrogenase_putative (ADH)	-2.493758657	-1.026187504	1.467571153
EHI_166490	C4M7F5	XP_652262.2	Alcohol dehydrogenase_putative (ADH)	-1.048881287	-1.286563624	-0.237682337
EHI_198620	C4LWQ8	XP_655201.2	PPi-PEPCK3	-8.318126762	-5.902664315	2.415462446
EHI_044970	Q9NH04	XP_648590.1	ME	-3.371544637	-2.282862579	1.088682059
EHI_014410	B1N2Y0	XP_001913546.1	MDH_putative	-2.539964263	-1.29009284	1.249871423
EHI_070720	C4M5S9	XP_654310.1	L-myo-inositol-1-phosphate synthase	-5.862557542	-4.718114024	1.144443518
Not detected						
EHI_161010	B1N3H7	XP_001913743.1	Anaerobic G3PDH subunit A_putative	-	-	2.79771936
Cytoskeleton dynamics and parasite virulence						
Increased						
EHI_110180	C4LU72	XP_657028.1	Myosin heavy chain	1.742008798	1.915355481	0.173346683
EHI_111050	C4M5I6	XP_657596.1	ARP2	2.48265	1.660252011	-0.822397989
EHI_058090	C4M8B0	XP_651163.1	Ras family GTPase	2.231234072	1.425210378	-0.806023694
EHI_196940	C4LVB2	XP_653132.1	Heat-shock protein 90_putative	2.326638075	1.816849869	-0.509788206
EHI_133900	B1N3C7	XP_001913693.1	Galactose-inhibitable lectin 170 kDa subunit_putative (Gal/GalNAc lectin)	2.50643645	1.484150956	-1.022285494
Reduced						
EHI_105210	C4M126	XP_653931.1	F-BAR domain-containing protein	-1.174858759	-1.873880924	-0.699022165
EHI_094060	B1N322	XP_001913588.1	Actin-binding protein_putative (filamin)	-3.592858259	-4.086887697	-0.494029438
EHI_164430	C4M1S5	XP_648375.2	Actinin-like protein_putative (α -actinin 1)	-6.424663932	-5.410549507	1.014114425
EHI_199000	C4LWU6	XP_653283.1	Calponin homology domain protein_putative (α -actinin 2)	-5.42520244	-4.937989077	0.487213363
EHI_136150	C4M295	XP_655240.2	Adenylyl CAP	-3.26152685	-3.039265215	0.222261635
EHI_177990	C4M553	XP_651490.1	Leucine-rich repeat containing protein	-9.129552234	-4.675234233	4.454318001
EHI_167060	B1N309	XP_001913575.1	Rab GDP dissociation inhibitor	-2.913843088	-1.601375505	1.312467583
EHI_098280	C4LXB1	XP_653621.1	14-3-3 protein (EhP2)	-4.15541176	-3.696594368	0.458817392
EHI_006810	C4M0F4	XP_654465.1	14-3-3 protein 2 (EhP3)	-3.628432526	-4.653662911	-1.025230385
EHI_159160	C4LX20	XP_648827.1	SOD	-1.016518349	-1.037119891	-0.020601541
EHI_121620	B1N5Y9	XP_001914605.1	Peroxiredoxin_putative (PRDX)	-3.343027913	-2.14245569	1.200572222
EHI_156710	B1N502	XP_001914268.1	3-ketoacyl-CoA synthase 4_putative	-7.753320965	-5.739869952	2.013451013
EHI_199590	C4M770	XP_654737.1	70 kDa heat-shock protein_putative	-6.306522113	-6.50351067	-0.196988557
EHI_052860	C4M3S5	XP_650458.1	Heat-shock protein 70_putative	-5.496325809	-5.150576387	0.345749422
Not detected						
EHI_187770	C4M9I2	XP_656019.2	SH3 domain protein	-	-	0.303916225
EHI_096420	C4LWF5	XP_656918.1	LIM zinc finger domain-containing protein (LimA)	-	-	-0.78774608
EHI_178470	C4LUR3	XP_653036.1	CPBP6	-	-	-0.611080228
Gene expression and protein modification						
Increased						
EHI_050130	C4LTQ0	XP_657191.1	60S ribosomal protein L14_putative	5.702363161	1.648304292	-4.054058869

Table 1. (Continued).

Gene ID	UniProt	NCBI	Protein description	EhCFIm25- dsRNA vs nontreated (control) (log2 fold change)	EhCFIm25- dsRNA vs <i>gfp</i> -dsRNA (log2 fold change)	<i>gfp</i> -dsRNA vs nontreated (control) (log2 fold change)
EHI_183480	C4M727	XP_654328.1	60S ribosomal protein L27_ putative	6.085963509	5.75025083	-0.335712679
EHI_166800	C4LY85	XP_654066.2	Ubiquitin_ putative	3.628806975	2.824287894	-0.804519081
Reduced						
EHI_006860	C4LU56	XP_650508.1	60S ribosomal protein L5_ putative	-5.900697969	-6.602091887	-0.701393918
EHI_064710	B1N384	XP_001913650.1	60S ribosomal protein L4_ putative	-4.30857207	-1.809131252	2.499440818
EHI_126920	C4LWV8	XP_651543.1	Asparaginyl-tRNA synthetase_ putative	-5.641036285	-2.595619356	3.045416929
EHI_073460	C4LXL0	XP_656678.1	Glycyl-tRNA synthetase_ putative	-5.479050074	-2.509932008	2.969118066
EHI_029530	B1N3R9	XP_001913834.1	60S ribosomal protein L7a_ putative	-4.111168396	-4.816620213	-0.705451818
EHI_175050	C4LZNO	XP_649894.1	Aspartyl-tRNA synthetase_ putative	-3.438382911	-2.571822649	0.866560262
EHI_166810	B1N306	XP_001913572.1	Elongation factor 2 (EF2)	-2.301951732	-1.132943057	1.169008675
EHI_011210	C4M7D4	XP_651869.1	Elongation factor 1 alpha (EF1- α)	-	-	-
EHI_090400	B1N2Z3	XP_001913560.1	60S acidic ribosomal protein P0	-2.115985101	-1.731688644	0.384296458
EHI_008380	C4M0L4	XP_652558.1	Aminopeptidase	-6.89523807	-2.603764161	4.291473908
EHI_153640	B1N2E5	XP_001913371.1	Protein kinase domain-containing protein	-3.876761502	-2.627397512	1.24936399
EHI_071590	C4MB38	XP_650651.1	Protein disulfide isomerase_ putative	-2.7241992	-3.178404428	-0.454205228
Not detected						
EHI_138770	C4M4I3	XP_650140.2	60S acidic ribosomal protein P2_ putative	-	-	-6.131527277
EHI_050280	C4LTO5	XP_648594.1	40S ribosomal protein S3a	-	-	1.176668332
EHI_199990	B1N442	XP_001913958.1	40S ribosomal protein S6	-	-	-1.587461998
EHI_150160	B1N3F1	XP_001913717.1	ATP-dependent RNA helicase DDX39_ putative	-	-	0.739544932
EHI_033250	C4M6Y2	XP_650900.1	Polyadenylate-binding protein_ putative (PABP)	-	-	-0.121076556
EHI_193350	C4M4T9	XP_651950.1	3' (2')_5'-bisphosphate nucleotidase_ putative	-	-	3.250181479

EhCFIm25 silencing affects cytoskeleton dynamics reducing parasite virulence

The cytoskeleton dynamics is essential for various cellular functions in *E. histolytica*, from cytokinesis to morphogenesis, including adhesion, endocytosis, phagocytosis, motility, and migration, that are pivotal activities in amoebic pathogenesis [23]. Although it is the key cytoskeletal protein, actin dynamics requires a coordinated cooperation with a large number of actin-binding proteins (ABPs) (including myosin II). Recently, a bioinformatic approach identified a total of 390 ABPs, most of them corresponding to uncharacterized proteins [24]. Here, we found that several proteins linked to the actin-rich cytoskeleton were modulated in EhCFIm25-silenced trophozoites. Notably, eight ABPs (C4M126, C4M9I2, B1N322, C4M1S5, C4LW6, C4M295, C4M553, and C4LWF5) were downregulated in *EhCFIm25*-silenced trophozoites. C4M126 (F-BAR domain-containing protein) and C4M9I2 (SH3 domain

protein) contain a BAR (bin-amphiphysin-Rvs) domain that has been involved in membrane curvature and actin binding. In *E. histolytica*, phagocytosis was inhibited by EhBAR (C4M128) silencing, indicating its participation in actin dynamics [25]. In addition, the SH3 domain is enriched in proteins that are upregulated in phagocytic trophozoites [26]. The atypical filamin (B1N322) [27], α -actinin 1 (C4M1S5) [28], and α -actinin 2 (C4LWU6) [29] are members of the calponin family that are able to cross-link actin to stimulate an active net; filamins, particularly filamin A also known as ABP120, have been localized in pseudopods and uropods [30], while α -actinin 2 (EhActn2) was involved in phagocytic cup formation [31]. The adenylyl cyclase-associated protein (C4M295) of the cyclase-associated protein (CAP) family is involved in actin remodeling [32] and nutritional response signaling [33]. The leucine-rich repeat containing protein (C4M553), an I/LWEQ domain-containing protein, has two leucine-rich repeats that are thought to promote protein

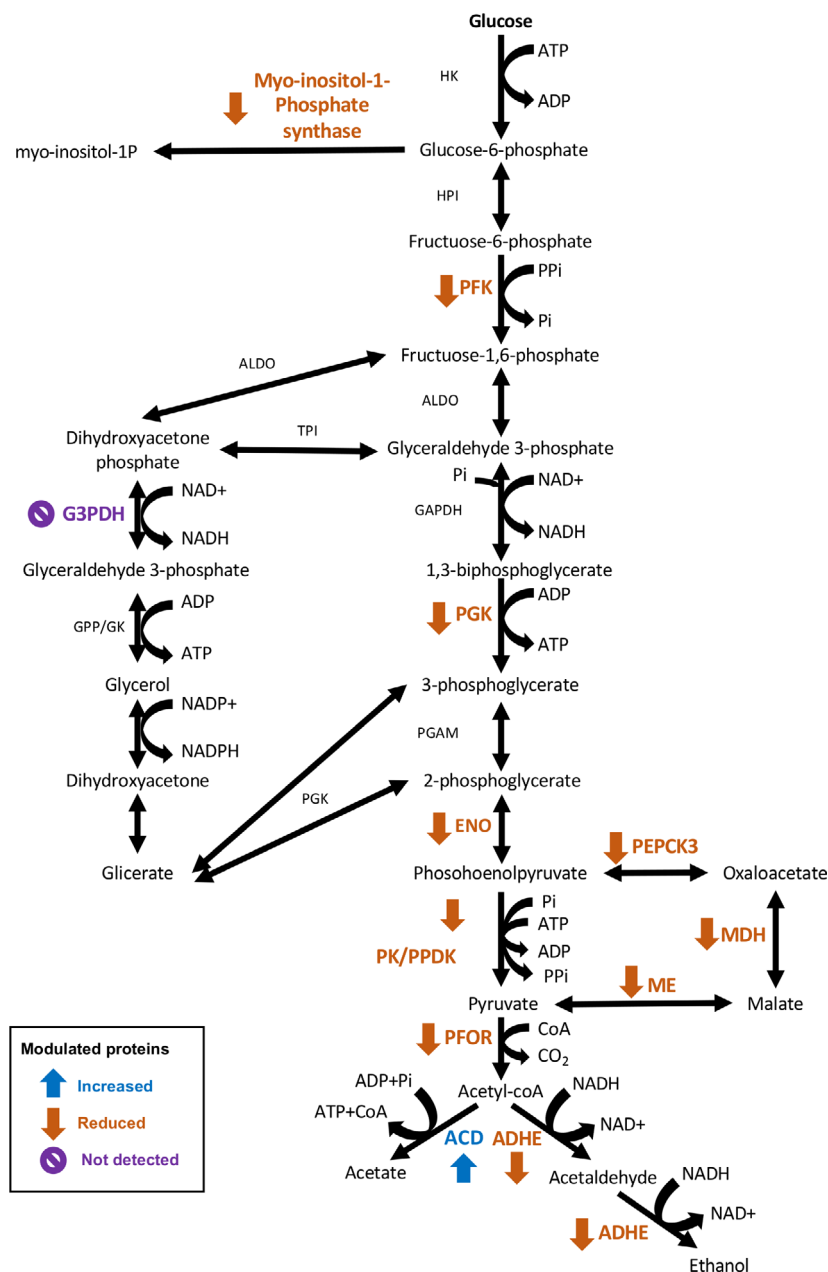


Fig. 6. Representation of protein changes in the atypical glycolysis of *E. histolytica* and related pathways in EhCFIm25-silenced trophozoites. Abbreviations are as follows: HK, hexokinase; HPI, phosphoglucose isomerase; PFKm phosphofructokinase; ALDO, aldolase; GAPDH, glyceraldehyde 3-phosphate dehydrogenase; PGK, phosphoglycerate kinase; PGAM, phosphoglycerate mutase; ENO, enolase; PK/PPDK, pyruvate, phosphate dikinase; PFOR, pyruvate ferredoxin oxidoreductase; ADHE, aldehyde-alcohol dehydrogenase; ACD, acetyl-CoA synthetase (ADP forming); PEPCK3, phosphoenolpyruvate carboxykinase; MDH, malate dehydrogenase; ME, malic enzyme; TPI, triosephosphate isomerase; G3PDH, glyceral-3-phosphate dehydrogenase; GPP/GK, glycerol-3-phosphate phosphatase/ glycerol kinase.

interactions with surface proteins [34] and a FERM domain that links cytoskeleton proteins to the plasma membrane [35]. EhLimA (C4LWF5) is a LIM domain-containing protein that colocalized to the plasma membrane with actin filaments in *E. histolytica* [36]. These alterations in ABP amount can be related to the reduced abundance of a small Ras family GTPase (C4M8B0) and a Rab GDP dissociation inhibitor (B1N309) known to regulate the GDP-GTP exchange reaction of members of the Rab family, leading to a reduction in vesicular trafficking.

On the other hand, only two cytoskeletal-related proteins were found with an increased abundance: the heavy chain of myosin II (C4LU72) which binds F-actin and is responsible for cell contraction and motility [37] and ARP2 (C4M5I6), one of the seven subunits of the ARP2/3 complex that mediates actin nucleation and has been localized in phagosomes [38]. Globally, changes observed in the abundance of these cytoskeletal proteins likely affect cytoskeleton organization and dynamics, which can be related to the augmented size of trophozoites and the increased number

of nuclei in *EhCFIm25*-silenced trophozoites, probably due to failure in cytokinesis; cytoskeleton alterations could also be responsible for the reduced mobility and erythrophagocytosis capacity in trophozoites, affecting their virulence capacity [14].

Congruently with these observations, our results evidenced the downregulation of other proteins previously related to phagocytosis, an essential process for parasite nutrition and pathogenesis. Members of the cysteine protease-binding protein family (CPBF), a single-transmembrane carrier/receptor family, interact with lysosomal hydrolytic enzymes and regulate their trafficking; notably, CPBF6 (C4LUR3) was identified in phagosomes, participating in the transport of cargo proteins, namely α -amylase and γ -amylase [39]. EhP3 (C4M0F4), a homolog of 14-3-3 family of protein, participates in initiation/formation of phagocytic cups and formation of phagosome, by acting as an adaptor molecule to recruit proteins that allow dynamics of F-actin rearrangement during phagocytosis [40]. Several heat-shock proteins (HSP) have also been involved in parasite virulence; notably, the activity of HSP70 is necessary for amoebic liver abscess formation in hamsters [41], while HSP90 controls the process of phagocytosis [42]. Then, the modulation of HSP90 (CELVB2) and HSP70 (C4M770, C4M3S5) could contribute to the reduced virulence capacity of *EhCFIm25*-silenced parasites. In addition to phagocytosis, the virulence process of *E. histolytica* includes adherence to target cells, cytolysis, and evasion of host immune response with the participation of various key proteins [43]. Therefore, the reduced amount of the galactose-inhibitable lectin 170 kDa subunit (B1N3C7) (Gal/GalNAc lectin) located on the surface of trophozoite contributes to reduce adherence to galactose and N-acetylgalactosamine of host cells. Moreover, we also found lower amount of peroxiredoxin (B1N5Y9) (PRX) and superoxide dismutase (SOD) (C4LX20), two enzymes involved in resistance of host oxidative defenses, that are important components of amoebic virulence [44]. The reduced amount of 3-ketoacyl-CoA synthase 4 or fatty acid elongase (B1N502) could also have an impact on parasite virulence properties that require an active lipid membrane dynamic [45].

***EhCFIm25* silencing has an impact on gene expression**

The last group of proteins with an altered amount in *EhCFIm25*-silenced trophozoites can be generally clustered around gene expression and protein modifications, which may explain the proteomic changes described above that promotes parasite death and

virulence diminution. Most of these proteins showed a reduced abundance or were not detected, in agreement with the high number of downregulated proteins. They include several ribosomal proteins (C4LU56, B1N384, B1N3R9, B1N2Z3, C4M4I3, C4LTQ5, B1N442), aminoacyl-tRNA synthetases (C4LWW8, C4LXL0, C4LZN0), elongation factors (C4M7D4, B1N306), and an aminopeptidase (C4M0L4), a protein kinase domain-containing protein (B1N2E5) and a protein disulfide isomerase (C4MB38). Additionally, two proteins that are important for RNA metabolism were not detected: the ATP-dependent RNA helicase DDX39 (B1N3F1) whose homologue in humans participates in the regulation of transcription, splicing, and RNA export [46] and the polyadenylate-binding protein_putative (C4M6Y2) that interacts with the PAP to enhance polyadenylation at the 3'-end of mRNA and bind the poly(A) tail to avoid transcript degradation and promotes translation through mRNA circularization and interaction with eIF4G [47]. Altogether, our results demonstrate that the absence of *EhCFIm25* had an impact on gene expression and proteome, and as a result, on *E. histolytica* survival and virulence properties, however, the molecular mechanisms involved remain unclear. In our previous work, we showed that *EhCFIm25* controls the efficient selection of distal (or downstream) poly(A) sites in *E. histolytica* transcripts and hypothesized that its silencing may have an impact on the 3'-end mRNA processing and therefore gene expression of the 20 identified genes with two polyadenylation sites [14,48]. Surprisingly, proteins that are modulated in our proteomics analysis did not correspond to any of these genes, which agrees with the limited impact of alternative polyadenylation on gene expression regulation in this parasite. In humans, CFIm25 is also essential for polyadenylation factors recruitment, pre-mRNA cleavage, and poly(A) tail synthesis [4–7]. Therefore, it is possible that changes in protein abundance following *EhCFIm25* silencing may result more from alterations in these events that from an upstream shift in poly(A) site selection; future experiments required to be performed to confirm this assumption. On the other hand, it is important to point out that a proteome does not represent the full set of proteins expressed in a cell, and it is an approximation that depends on the identification of peptides and their amount; moreover, the shotgun analysis presented here has been performed in total protein extracts, which may limit the detection of less abundant proteins. Notably, several genes with two poly(A) sites correspond to nuclear proteins that participate in DNA condensation, DNA binding, translation, splicing, and mRNA binding; similarly, the

nuclear EhCFIm25 protein was not identified in any of the three proteomes. The absence of nuclear proteins among the identified proteins is likely related to the lower amount of nuclear proteins in comparison with cytoplasmic proteins. It is possible that a proteomic analysis of nuclear proteins would give some insights about the abundance of these specific proteins. Additionally, the increased expression of EhPAP and EhPC4 that interact with EhCFIm25 suggests the existence of compensatory mechanisms in gene expression regulation that may help to overcome the absence of EhCFIm25 and reduce, at least partially, alterations in transcription and RNA processing, for parasite survival during the first days.

In conclusion, the present proteomic approach confirmed the significance of EhCFIm25 as a biochemical target in *E. histolytica* by providing interesting insights about the proteins and biological pathways that are altered following the absence of this polyadenylation factor. Notably, our results suggested that EhCFIm25 silencing affected energy metabolism and cytoskeleton dynamics causing parasite death and reducing parasite virulence, respectively, by altering gene expression, which explains parasite death, and alteration in virulence properties that were observed in the absence of EhCFIm25. The next step will involve additional studies to confirm the hypotheses emerging from our proteomic analysis and get a comprehensive view of the molecular mechanisms involved.

Acknowledgements

RGAB and this work were supported by SEP/CONACyT/Mexico (grant number 285467). ERM and LAM were supported by COFAA-IPN and EDI-IPN. AISM was a BEIFI-IPN (20180594 and 20194920) and CONACyT fellowship (Mexico). The authors thank Emmanuel Ríos Castro from the Unidad de Genómica, Proteómica y Metabólica (LaNSE; CINVESTAV-Unidad Ciudad de México, México) for performing the analysis of LC-ESI-HDMSE. The mass spectrometry proteomic data have been deposited to the ProteomeXchange Consortium via the PRIDE [49] partner repository with the dataset identifier PXD027784 and 10.6019/PXD027784. The funders had no role in the design of the study; in the collection, analyses, or interpretation of data; in the writing of the manuscript; or in the decision to publish the results.

Conflict of interest

The authors declare no conflict of interest.

Author contributions

LAM and CLC conceived and supervised the study; LAM and ERM designed experiments; AISM and RGAB performed experiments and bioinformatics analyses; CACS provided new strategies and reagents; RGAB and ERM analyzed data; LAM, AISM, and RGAB wrote the manuscript; ERM, CLC, and CACS made manuscript revisions.

Data accessibility

The data that support the findings of this study are openly available in the ProteomeXchange Consortium at <http://www.proteomexchange.org/>, reference number PXD027784.

References

- Shirley DT, Watanabe K and Moonah S (2019) Significance of amebiasis: 10 reasons why neglecting amebiasis might come back to bite us in the gut. *PLoS Negl Trop Dis* **13**, e0007744.
- Valdés-Flores J, López-Rosas I, López-Camarillo C, Ramírez-Moreno E, Ospina-Villa JD and Marchat LA (2018) Life and death of mRNA molecules in *Entamoeba histolytica*. *Front Cell Infect Microbiol* **8**, 199.
- Ospina-Villa JD, Tovar-Ayona BJ, López-Camarillo C, Soto-Sánchez J, Ramírez-Moreno E, Castañón-Sánchez CA and Marchat LA (2020) mRNA polyadenylation machineries in intestinal protozoan parasites. *J Eukaryot Microbiol* **67**, 306–320.
- Brown KM and Gilmartin GM (2003) A mechanism for the regulation of pre-mRNA 3' processing by human cleavage factor Im. *Mol Cell* **12**, 1467–1476.
- Kim S, Yamamoto J, Chen Y, Aida M, Wada T, Handa H and Yamaguchi Y (2010) Evidence that cleavage factor Im is a heterotetrameric protein complex controlling alternative polyadenylation. *Genes Cells* **15**, 1003–1013.
- Li H, Tong S, Li X, Shi H, Ying Z, Gao Y, Ge H, Niu L and Teng M (2011) Structural basis of pre-mRNA recognition by the human cleavage factor Im complex. *Cell Res* **21**, 1039–1051.
- Yang Q, Coseno M, Gilmartin GM and Doublé S (2011) Crystal structure of a human cleavage factor CFIm25/CFIm68/RNA complex provides an insight into poly(A) site recognition and RNA looping. *Structure* **19**, 368–377.
- Pezet-Valdez M, Fernández-Retana J, Ospina-Villa JD, Ramírez-Moreno ME, Orozco E, Charcas-López S, Soto-Sánchez J, Mendoza-Hernández G, López-Casamicha M, López-Camarillo C *et al.* (2013) The 25 kDa subunit of cleavage factor Im is a RNA-binding

- protein that interacts with the poly(A) polymerase in *Entamoeba histolytica*. *PLoS ONE* **8**, e67977.
- 9 Hernandez de la Cruz O, Muñoz-Lino M, Guillén N, Weber C, Marchat LA, López-Rosas I, Ruiz-García E, Astudillo-de la Vega H, Fuentes-Mera L, Álvarez-Sánchez E *et al.* (2014) Proteomic profiling reveals that EhPC4 transcription factor induces cell migration through up-regulation of the 16-kDa actin-binding protein EhABP16 in *Entamoeba histolytica*. *J Proteomics* **111**, 46–58.
 - 10 Hernández de la Cruz O, Marchat LA, Guillén N, Weber C, López Rosas I, Díaz-Chávez J, Herrera L, Rojo-Domínguez A, Orozco E and López-Camarillo C (2016) Multinucleation and polykaryon formation is promoted by the EhPC4 transcription factor in *Entamoeba histolytica*. *Sci Rep* **6**, 19611.
 - 11 Ospina-Villa JD, Zamorano-Carrillo A, Lopez-Camarillo C, Castañon-Sanchez CA, Soto-Sanchez J, Ramirez-Moreno E and Marchat LA (2015) Amino acid residues Leu135 and Tyr236 are required for RNA binding activity of CFIm25 in *Entamoeba histolytica*. *Biochimie* **115**, 44–51.
 - 12 Ospina-Villa JD, García-Contreras J, Rosas-Trigueros JL, Ramírez-Moreno E, López-Camarillo C, Zamora-López B, Marchat LA and Zamorano-Carrillo A (2018) Importance of amino acids Leu135 and Tyr236 for the interaction between EhCFIm25 and RNA: a molecular dynamics simulation study. *J Mol Model* **24**, 202.
 - 13 Ospina-Villa JD, Dufour A, Weber C, Ramirez-Moreno E, Zamorano-Carrillo A, Guillen N, Lopez-Camarillo C and Marchat LA (2018) Targeting the polyadenylation factor EhCFIm25 with RNA aptamers controls survival in *Entamoeba histolytica*. *Sci Rep* **8**, 5720.
 - 14 Ospina-Villa JD, Guillén N, Lopez-Camarillo C, Soto-Sanchez J, Ramirez-Moreno E, Garcia-Vazquez R, Castañon-Sanchez CA, Betanzos A and Marchat LA (2017) Silencing the cleavage factor CFIm25 as a new strategy to control *Entamoeba histolytica* parasite. *J Microbiol* **55**, 783–791.
 - 15 Diamond LS, Harlow DR and Cunnick CC (1978) A new medium for the axenic cultivation of *Entamoeba histolytica* and other *Entamoeba*. *Trans R Soc Trop Med Hyg* **72**, 431–432.
 - 16 Silva JC, Gorenstein MV, Li GZ, Vissers JP and Geromanos SJ (2006) Absolute quantification of proteins by LCMSE: a virtue of parallel MS acquisition. *Mol Cell Proteomics* **5**, 144–156.
 - 17 Félix-Contreras C, Alba-Fierro CA, Ríos-Castro E, Luna-Martínez F, Cuéllar-Cruz M and Ruiz-Baca E (2020) Proteomic analysis of *Sporothrix schenckii* cell wall reveals proteins involved in oxidative stress response induced by menadione. *Microb Pathog* **141**, 103987.
 - 18 Ramírez-Flores CJ, Cruz-Mirón R, Mondragón-Castelán ME, González-Pozos S, Ríos-Castro E and Mondragón-Flores R (2019) Proteomic and structural characterization of self-assembled vesicles from excretion/secretion products of *Toxoplasma gondii*. *J Proteomics* **208**, 103490.
 - 19 Penuliar GM, Furukawa A, Nakada-Tsukui K, Husain A, Sato D and Nozaki T (2012) Transcriptional and functional analysis of trifluoromethionine resistance in *Entamoeba histolytica*. *J Antimicrob Chemother* **67**, 375–386.
 - 20 Jones CP and Ingram-Smith C (2014) Biochemical and kinetic characterization of the recombinant ADP-forming acetyl coenzyme A synthetase from the amitochondriate protozoan *Entamoeba histolytica*. *Eukaryot Cell* **13**, 1530–1537.
 - 21 Loftus B, Anderson I, Davies R, Alsmark UC, Samuelson J, Amedeo P, Roncaglia P, Berriman M, Hirt RP, Mann BJ *et al.* (2005) The genome of the protist parasite *Entamoeba histolytica*. *Nature* **433**, 865–868.
 - 22 Pineda E, Encalada R, Vázquez C, Néquiz M, Olivos-García A, Moreno-Sánchez R and Saavedra E (2015) In vivo identification of the steps that control energy metabolism and survival of *Entamoeba histolytica*. *FEBS J* **282**, 318–331.
 - 23 Manich M, Hernandez-Cuevas N, Ospina-Villa JD, Syan S, Marchat LA, Olivo-Marin JC and Guillén N (2018) Morphodynamics of the Actin-Rich Cytoskeleton in *Entamoeba histolytica*. *Front Cell Infect Microbiol* **8**, 179.
 - 24 Rath PP and Gourinath S (2020) The actin cytoskeleton orchestra in *Entamoeba histolytica*. *Proteins* **88**, 1361–1375.
 - 25 Sateriale A, Miller P and Huston CD (2016) Knockdown of five genes encoding uncharacterized proteins inhibits *Entamoeba histolytica* phagocytosis of dead host cells. *Infect Immun* **84**, 1045–1053.
 - 26 Sateriale A, Vaithilingam A, Donnelly L, Miller P and Huston CD (2012) Feed-forward regulation of phagocytosis by *Entamoeba histolytica*. *Infect Immun* **80**, 4456–4462.
 - 27 Hon CC, Nozaki T and Guillén N (2010). Dissecting the Actin cytoskeleton of *Entamoeba histolytica* from a genomic perspective. In *Anaerobic Parasitic Protozoa: Genomics and Molecular Biology* (Clark CG, Johnson PJ and Adam RD, eds), pp. 81–118. Caister Academic Press, Norfolk, United Kingdom.
 - 28 Virel A and Backman L (2004) Molecular evolution and structure of alpha-actinin. *Mol Biol Evol* **21**, 1024–1031.
 - 29 Virel A, Addario B and Backman L (2007) Characterization of *Entamoeba histolytica* alpha-actinin2. *Mol Biochem Parasitol* **154**, 82–89.
 - 30 Vargas M, Sansonetti P and Guillén N (1996) Identification and cellular localization of the actin-binding protein ABP-120 from *Entamoeba histolytica*. *Mol Microbiol* **22**, 849–857.

- 31 Pinotsis N, Zielinska K, Babuta M, Arolas JL, Kostan J, Khan MB, Schreiner C, Salmazo A, Ciccarelli L, Puchinger M *et al.* (2020) Calcium modulates the domain flexibility and function of an α -actinin similar to the ancestral α -actinin. *Proc Natl Acad Sci USA* **117**, 22101–22112.
- 32 Hubberstey AV and Mottillo EP (2002) Cyclase-associated proteins: CAPacity for linking signal transduction and actin polymerization. *FASEB J* **16**, 487–499.
- 33 Iwase S and Ono S (2016) The C-terminal dimerization motif of cyclase-associated protein is essential for actin monomer regulation. *Biochem J* **473**, 4427–4441.
- 34 Kobe B and Kajava AV (2001) The leucine-rich repeat as a protein recognition motif. *Curr Opin Struct Biol* **11**, 725–732.
- 35 Chishti AH, Kim AC, Marfatia SM, Lutchnan M, Hanspal M, Jindal H, Liu SC, Low PS, Rouleau GA, Mohandas N *et al.* (1998) The FERM domain: a unique module involved in the linkage of cytoplasmic proteins to the membrane. *Trends Biochem Sci* **23**, 281–282.
- 36 Wender N, Villalobo E and Mirelman D (2007) EhLimA, a novel LIM protein, localizes to the plasma membrane in *Entamoeba histolytica*. *Eukaryot Cell* **6**, 1646–1655.
- 37 Arhets P, Olivo JC, Gounon P, Sansonetti P and Guillén N (1998) Virulence and functions of myosin II are inhibited by overexpression of light meromyosin in *Entamoeba histolytica*. *Mol Biol Cell* **9**, 1537–1547.
- 38 Marion S, Laurent C and Guillén N (2005) Signalization and cytoskeleton activity through myosin IB during the early steps of phagocytosis in *Entamoeba histolytica*: a proteomic approach. *Cell Microbiol* **7**, 1504–1518.
- 39 Furukawa A, Nakada-Tsukui K and Nozaki T (2013) Cysteine protease-binding protein family 6 mediates the trafficking of amylases to phagosomes in the enteric protozoan *Entamoeba histolytica*. *Infect Immun* **81**, 1820–1829.
- 40 Agarwal S, Anand G, Sharma S, Parimita Rath P, Gourinath S and Bhattacharya A (2019) EhP3, a homolog of 14–3–3 family of protein participates in actin reorganization and phagocytosis in *Entamoeba histolytica*. *PLoS Pathog* **15**, e1007789.
- 41 Santos F, Nequiz M, Hernández-Cuevas NA, Hernández K, Pineda E, Encalada R, Guillén N, Luis-García E, Saralegui A, Saavedra E *et al.* (2015) Maintenance of intracellular hypoxia and adequate heat shock response are essential requirements for pathogenicity and virulence of *Entamoeba histolytica*. *Cell Microbiol* **17**, 1037–1051.
- 42 Singh M, Sharma S, Bhattacharya A and Tatu U (2015) Heat Shock Protein 90 regulates encystation in *Entamoeba*. *Front Microbiol* **6**, 1125.
- 43 Betanzos A, Bañuelos C and Orozco E (2019) Host invasion by pathogenic amoebae: epithelial disruption by parasite proteins. *Genes* **10**, 618.
- 44 Davis PH, Zhang X, Guo J, Townsend RR and Stanley SL Jr (2006) Comparative proteomic analysis of two *Entamoeba histolytica* strains with different virulence phenotypes identifies peroxiredoxin as an important component of amoebic virulence. *Mol Microbiol* **61**, 1523–1532.
- 45 Castellanos-Castro S, Bolaños J and Orozco E (2020) Lipids in *Entamoeba histolytica*: host-dependence and virulence factors. *Front Cell Infect Microbiol* **10**, 75.
- 46 Sugiura T, Sakurai K and Nagano Y (2007) Intracellular characterization of DDX39, a novel growth-associated RNA helicase. *Exp Cell Res* **313**, 782–790.
- 47 Jenal M, Elkon R, Loayza-Puch F, van Haaften G, Kühn U, Menzies FM, Oude Vrielink JA, Bos AJ, Drost J, Rooijers K *et al.* (2012) The poly(A)-binding protein nuclear 1 suppresses alternative cleavage and polyadenylation sites. *Cell* **149**, 538–553.
- 48 Hon CC, Weber C, Sismeiro O, Proux C, Koutero M, Deloger M, Das S, Agrahari M, Dillies MA, Jagla B *et al.* (2013) Quantification of stochastic noise of splicing and polyadenylation in *Entamoeba histolytica*. *Nucleic Acids Res* **41**, 1936–1952.
- 49 Perez-Riverol Y, Csordas A, Bai J, Bernal-Llinares M, Hewapathirana S, Kundu DJ, Inuganti A, Griss J, Mayer G, Eisenacher M *et al.* (2019) The PRIDE database and related tools and resources in 2019: improving support for quantification data. *Nucleic Acids Res* **47** (D1), D442–D450.

Supporting information

Additional supporting information may be found online in the Supporting Information section at the end of the article.

Fig S1. Effect of EhCFIm25 silencing on *E. histolytica* trophozoites proliferation and viability. Trophozoites (5.0×10^4) were soaked with *EhCFIm25*-dsRNA ($100 \mu\text{L}\cdot\text{mL}^{-1}$) at 37 °C. At day 4, total RNA was obtained to evaluate *EhCFIm25* mRNA expression by Real-time quantitative reverse transcription polymerase chain reaction (Real-time qPCR). The *EhRNAPII* gene mRNA expression was determined and used as normalization control. Data corresponding to the *EhCFIm25*-dsRNA condition were compared to both control conditions using the paired Student's *t*-test. $**P < 0.01$; $***P < 0.001$ (A). Each day, cells were counted (B) and parasite viability was assessed by the Trypan blue assay (C). Data corresponding to the *EhCFIm25*-dsRNA condition were compared to both control conditions using the two-way ANOVA test.

* $P < 0.05$ and *** $P < 0.001$. $n = 3$. Error bars represent SD.

Fig S2. Real-time quantitative reverse transcription polymerase chain reaction (Real-time qRT-PCR) for EhPAP and EhPC4 genes in EhCFIm25-dsRNA trophozoites compared with (A) non-treated cells and (B) gfp-dsRNA treated parasites. The EhRNAPII gene

mRNA expression was determined and used as normalization control for all qRT-PCR assays. Data corresponding to the EhCFIm25-dsRNA condition were compared to both control conditions using the paired Student's *t*-test. * $P < 0.05$; *** $P < 0.001$. $n = 3$. Error bars represent SD.

Table S1. Raw data.